

# Fixed-Length Dense Fingerprint Representation

Zhiyu Pan<sup>✉</sup>, Xiongjun Guan<sup>✉</sup>, Yongjie Duan<sup>✉</sup>, Jianjiang Feng<sup>✉</sup>, Member, IEEE, and Jie Zhou<sup>✉</sup>, Fellow, IEEE

**Abstract**—Fixed-length fingerprint representations, which map each fingerprint to a compact and fixed-size feature vector, are computationally efficient and well-suited for large-scale matching. However, designing a robust representation that effectively handles diverse fingerprint modalities, pose variations, and noise interference remains a significant challenge. In this work, we propose a fixed-length dense descriptor of fingerprints, and introduce FLARE—a fingerprint matching framework that integrates the Fixed-Length dense descriptor with pose-based Alignment and Robust Enhancement. This fixed-length representation employs a three-dimensional dense descriptor to effectively capture spatial relationships among fingerprint ridge structures, enabling robust and locally discriminative representations. To ensure consistency within this dense feature space, FLARE incorporates pose-based alignment using complementary estimation methods, along with dual enhancement strategies that refine ridge clarity while preserving the original fingerprint modality. The proposed dense descriptor supports fixed-length representation while maintaining spatial correspondence, enabling fast and accurate similarity computation. Extensive experiments demonstrate that FLARE achieves superior performance across rolled, plain, latent, and contactless fingerprints, significantly outperforming existing methods in cross-modality and low-quality scenarios. Further analysis validates the effectiveness of the dense descriptor design, as well as the impact of alignment and enhancement modules on the accuracy of dense descriptor matching. Experimental results highlight the effectiveness and generalizability of FLARE as a unified and scalable solution for robust fingerprint representation and matching. The implementation and code will be publicly available at our GitHub repository.

**Index Terms**—Fingerprint recognition, fixed-length fingerprint representation, dense descriptor, fingerprint enhancement, pose-based alignment.

## I. INTRODUCTION

**FINGERPRINT** as a biometric trait has several notable advantages, including ease of acquisition, high permanence, and enhanced privacy, making it broadly applicable in civilian and commercial fields [1]. A typical fingerprint recognition system comprises three key components: image acquisition, feature extraction, and matching [2]. Acquisition methods and modalities vary significantly across different application scenarios and are commonly classified as rolled, plain, latent, and contactless fingerprints. Consequently, robust and efficient feature extraction and matching algorithms are essential to ensure reliable recognition performance across varying acquisition conditions and fingerprint types. Initial research in fingerprint recognition primarily focused on designing handcrafted descriptors using level-1 (e.g., orientation field, frequency map)

This work was supported in part by the National Natural Science Foundation of China under Grant 62376132 and 62321005. (Corresponding author: Jianjiang Feng.)

The authors are with Department of Automation, Tsinghua University, Beijing 100084, China (e-mail: pzy20@mails.tsinghua.edu.cn; gxj21@mails.tsinghua.edu.cn; duanyj13@tsinghua.org.cn; jfeng@tsinghua.edu.cn; jzhou@tsinghua.edu.cn).

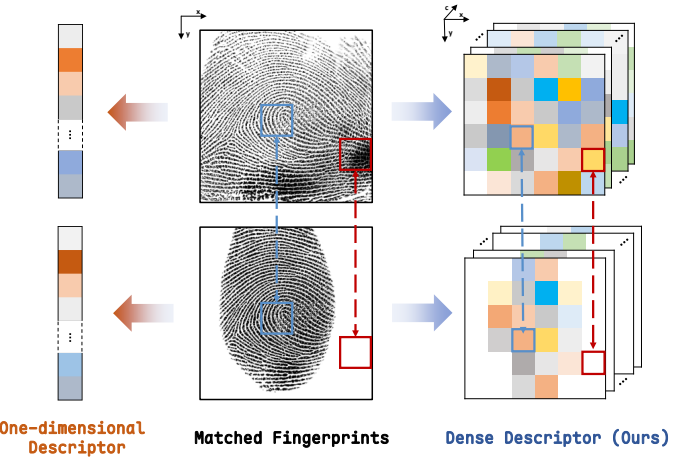


Fig. 1. Comparison of one-dimensional and dense descriptors. One-dimensional descriptors lose spatial structural information, whereas dense descriptors maintain spatial correspondence, enhancing local sensitivity and discriminative power while mitigating background noise.

and level-2 (e.g., ridge skeleton map, minutiae) fingerprint features [3]–[7]. However, these conventional methods often struggle with partial or noisy fingerprints and exhibit limited generalization across fingerprint modalities. Benefiting from the efficiency and strong discriminative power of deep feature learning, deep learning has become the dominant paradigm in modern fingerprint matching systems.

We categorize fingerprint matching methods based on deep learning into three types. The first is pairwise matching networks, which take two fingerprint images as input and directly produce a similarity score by jointly processing their features [8]–[10]. While this enables fine-grained comparisons and high accuracy, the joint processing is computationally expensive and unsuitable for large-scale identification. The second category is local representation matching, where local descriptors are extracted from patches centered at detected minutiae or estimated orientation fields [11]–[13]. Each fingerprint is represented by a variable-length set of descriptors, and matching is performed by computing pairwise similarities. Although this method offers good accuracy, its efficiency is limited by the variable-length nature of the representation. The third is fixed-length representation matching, where a neural network encodes each fingerprint into a global fixed-length feature vector [14]–[17]. This allows for fast, many-to-many comparisons via matrix operations, making it highly efficient and scalable for large-scale matching. Nonetheless, the matching accuracy of fixed-length representations tends to degrade in challenging scenarios, such as latent fingerprints or partial and low-quality impressions with missing or distorted ridge structures [18]. Motivated by these observations, we present FLARE — a fingerprint matching framework that com-

bines a Fixed-Length dense descriptor with pose-based ridge Alignment and Robust Enhancement. Our approach preserves the efficiency of fixed-length matching while significantly improving robustness and accuracy under challenging fingerprint conditions, thereby enhancing overall generalizability.

Most existing fixed-length methods represent fingerprint descriptors as one-dimensional vectors [16]–[18], which often fail to suppress interference from background regions (Fig. 1 left). As a result, their matching accuracy degrades when there are significant differences in fingerprint foreground areas or in the presence of strong background noise. Some approaches [19], [20] attempt to mitigate these challenges by incorporating foreground attention masks during representation learning or by dividing fingerprint images into multiple regions for feature extraction and fusion. However, these strategies operate at the feature or region level and do not explicitly suppress background interference or adapt to variations across different foreground areas at the descriptor level. To overcome these limitations, we build upon the form of dense representation [13] and proposed a fixed-length dense descriptor, which serves as a localized deep representation of the fingerprint in the form of a three-dimensional tensor, where two spatial dimensions align with the original image coordinates (Fig. 1 right). The dense descriptor is defined only within the fingerprint foreground region, while background areas are left empty, effectively eliminating background interference. When two fingerprints are spatially aligned, matching is performed only within the overlapping foreground regions of the dense descriptors, allowing the method to handle partial fingerprints more effectively. Therefore, the dense representation offers enhanced robustness in challenging scenarios such as low-quality or incomplete fingerprints.

Since dense descriptor matching relies on accurate spatial alignment, misalignment between fingerprint pairs can significantly degrade performance. To address this, FLARE adopts a pose-based alignment strategy built on 2D fingerprint pose estimation [21]–[25]. Each fingerprint is normalized into a unified coordinate system by aligning its estimated central location and orientation, requiring only a single transformation per image. This alignment strategy preserves the efficiency of fixed-length representation matching while enhancing robustness to pose variations. To improve alignment reliability under varying fingerprint quality and patterns, FLARE further integrates two complementary state-of-the-art pose estimation methods: the dense voting approach of Duan et al. [24] and the region detection-based regression method of Guan et al. [25]. The former aggregates local predictions from ridge-level features, while the latter directly regresses global pose from coarse structural cues. By combining these two approaches, FLARE leverages both fine-grained local details and global spatial structure to achieve more robust and consistent alignment across fingerprint modalities.

To support fixed-length dense fingerprint representation, enhancement plays a critical role in improving ridge clarity and suppressing background noise, thereby facilitating effective descriptor extraction and improving overall matching accuracy. However, many existing methods [26]–[29] transform fingerprint images into a new modality that retains only ridge

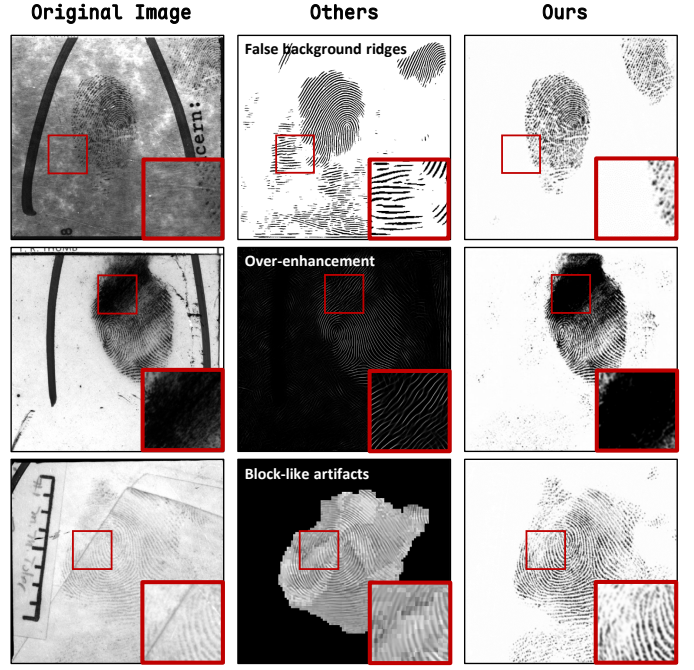


Fig. 2. Visual comparison of enhancement methods. Each row shows an original fingerprint (left), the result from a representative existing method (middle), and our enhancement (right). Compared to previous methods, which may hallucinate background ridges (top) [26], over-generate ridges in blurry regions (middle) [27], or exhibit block artifacts (bottom) [28], our approach preserves the original impression style, suppresses background interference, and avoids introducing spurious textures.

like structures. These approaches often rely on perceptual estimations of ridge patterns, which can be unreliable in noisy or low-quality regions. As a result, they may hallucinate artificial ridges or inadvertently remove valid fingerprint areas, reducing compatibility with descriptor networks. In contrast, our enhancement strategy directly operates on the original fingerprint texture, suppressing noise and improving contrast without altering ridge structures. This preserves structural fidelity and ensures compatibility with dense descriptor learning (Fig. 2). Drawing inspiration from LFRNet [18], we propose UNetEnh, a UNet-based model [30] trained on simulated low-quality fingerprints. In addition, we introduce PriorEnh, which leverages a VQ-VAE [31] to learn a latent ridge-structure codebook from high-quality fingerprints. This prior guides the enhancement process and enables partial ridge reconstruction in degraded regions. Experimental results show that PriorEnh improves matching across a variety of fingerprint types, while UNetEnh performs particularly well on latent fingerprints. To exploit their complementary strengths, FLARE combines both enhancement methods, leading to improved robustness and accuracy.

We conduct comprehensive experiments across multiple types of fingerprint datasets, demonstrating that FLARE consistently outperforms existing fixed-length methods in terms of matching accuracy. In addition, our enhancement strategy, which preserves the original image modality, achieves superior generalization and matching performance compared to previous enhancement approaches. Furthermore, the integration of multiple alignment and enhancement strategies is empirically

shown to further improve descriptor-level matching effectiveness. This work extends our previous conference paper FDD [32] by incorporating complementary pose estimation methods and introducing a set of newly designed fingerprint enhancement modules, along with a more comprehensive analysis of the fixed-length dense descriptor through additional experiments and ablation studies. Concretely, the contributions of this research are as follows:

- We propose a fixed-length dense descriptor and introduce FLARE—a fingerprint recognition framework centered on this representation. FLARE integrates pose-aware alignment and robust enhancement modules to improve both matching accuracy and generalizability across diverse fingerprint conditions.
- We design two enhancement modules, UNetEnh and PriorEnh, which operate directly on the original fingerprint texture to suppress background interference and enhance ridge clarity while preserving structural fidelity.
- We validate the effectiveness of the proposed dense descriptor through extensive experiments and ablation studies, and show that combining complementary alignment and enhancement strategies further improves descriptor-based fingerprint matching.

## II. RELATED WORK

### A. Fixed-length Fingerprint Representation

Fixed-length fingerprint representations encode an entire fingerprint image into a compact vector of fixed dimension, allowing similarity computation via distance metrics. With the rise of deep learning, fixed-length representations have become more robust and discriminative. Song and Feng [33] proposed integrating multi-scale representations from pyramid deep convolutional features. Cao et al. [14] introduced Spatial Transformer Networks (STNs) to assist fingerprint rectification. Engelsma et al. [16] further integrated STNs with compact descriptor networks, incorporating minutiae-aware features. Grosz et al. [17] combined CNN and Transformer features under STN-based alignment to improve performance. However, these STNs are typically trained without ground-truth pose supervision, relying instead on matching losses. Gu et al. [19] addressed this by training a pose estimator with annotated 2D poses and extracting multi-scale features from different fingerprint regions. Another line of work seeks alignment-free representations by improving robustness to pose variations, such as fusing multiple local representations aligned using minutiae anchors [34] or applying minutiae-supervised pooling [35]. These approaches, however, often depend heavily on minutiae extraction, making them sensitive to minutiae quality and foreground availability. In contrast, FLARE adopts the proposed pose-supervised dense fixed-length representation, which addresses these limitations by preserving spatial correspondence and suppressing background noise, thereby enhancing robustness and matching accuracy.

### B. Fingerprint 2D Pose Estimation

Unlike other biometric traits such as face or palmprint, fingerprints lack stable anatomical landmarks for defining a 2D

pose. Early works [36]–[39] attempted to estimate pose based on singular points, ridge curvature, or contours, but the diversity of fingerprint patterns and sensitivity to ridge quality limited their generalization [1]. Following the pose definition of Si et al. [21], where the center and orientation are derived from ridge flow characteristics, existing pose estimation methods can be broadly categorized into two types: global regression-based [16], [22], [25] and local voting-based approaches [24], [40]. Regression-based methods estimate the overall pose from the entire image, while voting-based methods aggregate local predictions from fingerprint patches. In FLARE, we integrate a global regression-based estimator [25] with a local voting-based method [24] to leverage their complementary strengths for improving matching performance.

### C. Fingerprint Enhancement

Fingerprint enhancement improves ridge clarity and supports better matching, particularly for low-quality images. Classical methods often rely on Gabor filtering. Cappelli et al. [41] used adaptive Gabor filters for local orientation and frequency; Feng et al. [42] and Yang et al. [39] improved robustness by introducing global and local orientation dictionaries combined with pose estimation. With deep learning, Tang et al. [28] modeled Gabor filtering as learnable convolutions to enhance latent fingerprints. GAN-based approaches have also emerged: Huang et al. [29] adopted a PatchGAN to refine latent fingerprints; Zhu et al. [27] framed enhancement as a modality translation task using FOMFE [4] and minutiae supervision. These methods, while effective for traditional minutiae-based matching, often transform the fingerprint into a new modality focused solely on ridge perception. This transformation risks introducing hallucinated patterns that compromise the quality of global deep representation extraction. Moreover, such methods exhibit limited robustness to structural variations and noise artifacts. In contrast, we argue that fingerprint enhancement should operate within the original image modality, preserving structural fidelity while suppressing background noise and enhancing ridge contrast. Following this principle, we develop two complementary enhancement modules integrated in FLARE: UNetEnh, a denoising-based model, and PriorEnh, a prior-guided reconstruction model learned from high-quality fingerprints. Their fusion further improves robustness and matching performance across fingerprint modalities.

## III. METHODOLOGY

### A. Overview of FLARE

The overall fingerprint matching pipeline of FLARE is illustrated in Fig. 3. For each input fingerprint, FLARE first estimates the 2D pose using two complementary estimators and aligns the image into standardized spatial configurations according to each estimator's interpretation. The aligned images are then enhanced through two distinct strategies<sup>1</sup>, followed by descriptor extraction to produce four sets of

<sup>1</sup>The rationale for performing pose estimation prior to enhancement is discussed in Sec. V.

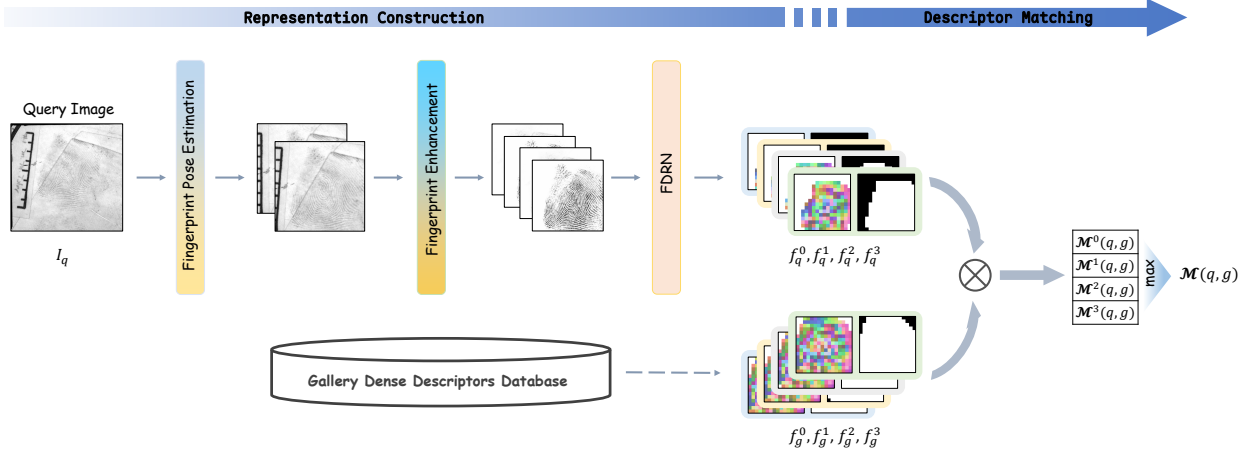


Fig. 3. FLARE matching pipeline. Each image is processed through two pose estimators and two enhancers, yielding four descriptor pairs. The final score is the maximum of four cosine similarities.

outputs, each consisting of a dense, fixed-length representation and a corresponding foreground mask. Matching between two fingerprints is performed by computing cosine similarity between descriptors within overlapping foreground regions. The four sets of descriptors are independently compared, yielding four similarity scores, and the maximum score is selected as the final matching result. The fingerprint pose estimation, enhancement, and dense descriptor extraction modules are trained independently. The following sections provide detailed descriptions of the pose estimation process, fingerprint enhancement, fixed-length dense descriptor extraction, and the matching procedure.

### B. Fingerprint 2D Pose Estimation

For fingerprint pose estimation, FLARE adopts a lightweight global regression-based method proposed by Guan et al. [25] and a local voting-based strategy proposed by Duan et al. [24]. The regression-based method predicts the fingerprint center and orientation directly from the overall fingerprint contour, while the voting-based method infers the pose by aggregating dense local predictions based on fine-grained ridge structures. By integrating both approaches, FLARE leverages complementary global and local information to achieve more reliable spatial alignment. Architectural and training details follow the original implementations.

To further enhance the robustness of pose estimation under background noise, we employ a data augmentation strategy that randomly inserts background patterns during training. This approach substantially improves performance on latent fingerprints with heavy background interference. In this part, background augmentation is performed using images from the MSRA-TD500 dataset [43].

### C. Fingerprint Enhancement

Our enhancement design aims to suppress background noise while enhancing the contrast of foreground ridge patterns. To train the enhancement network, we use optically captured high-quality fingerprints and simulate low-quality inputs through a set of handcrafted degradations. These include:

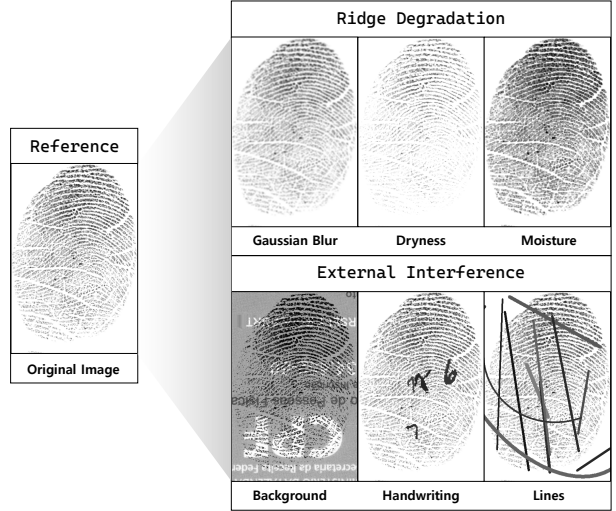


Fig. 4. Examples of fingerprint degradation simulation.

(1) ridge degradation, such as Gaussian blur, dry or moist fingerprint artifacts that reduce ridge quality; and (2) external interference, such as background overlays from BID [44] and occlusions with line patterns or handwritten digits from MNIST [45]. These degradations can be combined to increase diversity. Fig. 4 shows examples of high-quality fingerprints and their corresponding degraded versions. This process produces paired training samples  $(I_{LQ}, I_{HQ})$  for learning the enhancement network.

To enhance fingerprint quality while preserving structural fidelity, we propose two complementary modules: UNetEnh, a U-Net-based model that directly suppresses image noise, and PriorEnh, which incorporates ridge-structure priors to guide enhancement. UNetEnh adopts the U-Net architecture [30], taking simulated noisy fingerprints  $I_{LQ}$  as input and producing enhanced outputs  $I_{Enh}$ . PriorEnh is trained in two stages (Fig. 5). In the first stage, a VQ-VAE [31] is trained in a self-reconstruction manner using high-quality fingerprints  $I_{HQ}$  to learn a latent codebook  $\mathcal{C} \in \mathbb{R}^{l_c \times d_c}$  that captures fine-grained ridge priors. In the second stage, the pretrained

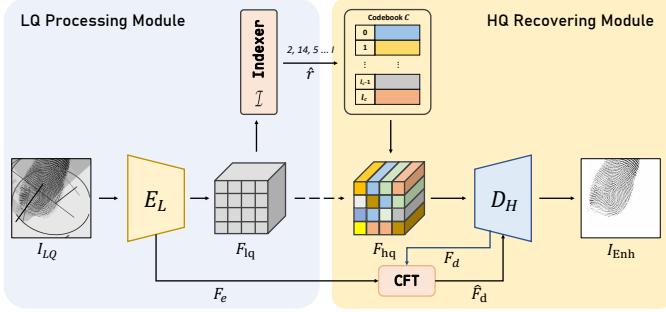


Fig. 5. The architecture illustration of PriorEnh.

codebook  $\mathcal{C}$  and decoder  $D_H$  are frozen. A U-Net-shaped encoder  $E_L$ , a GatedPixelCNN-based indexer  $\mathcal{I}$  [46], and a controllable feature transformation (CFT) module [47] are jointly trained with  $I_{LQ}$  as input and  $I_{HQ}$  as the target. The encoder and indexer reconstruct latent representations, while the CFT module modulates decoder features using spatial transformations from encoder activations, improving output fidelity.

To address the computational cost of operating on relatively large latent maps, we adopt GatedPixelCNN [46] as the indexer  $\mathcal{I}$  that produce the indexes to the codebook in a  $l_c$  classification form as  $\hat{r}$ . The CFT module enables the encoder features  $F_e$  to modulate the decoder features  $F_d$  through spatial feature transformation:

$$\hat{F}_d = F_d + (\alpha \odot F_d + \beta) \times w ; \quad \alpha, \beta = \text{CFT}(F_d, F_e) , \quad (1)$$

where  $\alpha$  and  $\beta$  are the affine parameters, and  $w \in [0, 1]$  is a weighting factor that controls the degree of influence. Together with the pretrained codebook and decoder from the first stage, these components constitute the full PriorEnh network.

The enhancement loss  $\mathcal{L}_{\text{Enh}}$  for UNetEnh can be simply calculated by the Mean Square Error (MSE) between the predicted enhanced fingerprint image  $I_{\text{Enh}}$  and  $I_{\text{HQ}}$ . In the case of PriorEnh, the first-stage training loss  $\mathcal{L}_{\text{Enh}}^{s1}$  is consistent with that of the standard VQ-VAE [31], and thus is not elaborated here. For the second training stage, we supervise the reconstruction of the latent feature map using the following loss:

$$\mathcal{L}_{\text{ind}} = \|F_{\text{Lq}} - \text{sg}(F_c)\|_2^2 + \lambda_{\text{ind}} \sum_{i=0}^{hw-1} -r_i^* \log(\hat{r}_i) , \quad (2)$$

where  $F_{\text{Lq}} \in \mathbb{R}^{h \times w \times d_c}$  denotes the latent feature map produced by the low-quality encoder  $E_L$ , and  $F_c$  is the corresponding latent feature map generated by the first-stage encoder  $E_H$  with high-quality input  $I_{\text{HQ}}$ . The operator sg indicates stop-gradient.  $\hat{r}_i$  denotes the predicted index probability of the  $i$ -th spatial location, and  $r_i^*$  is the corresponding ground truth generated from  $F_c$ . We set  $\lambda_{\text{ind}} = 0.5$  in our case. The total loss for the second training stage is defined as:

$$\mathcal{L}_{\text{Enh}}^{s2} = \|I_{\text{Enh}} - I_{\text{HQ}}\|_1 + \|\mathcal{P}(I_{\text{Enh}}) - \mathcal{P}(I_{\text{HQ}})\|_2^2 + \mathcal{L}_{\text{ind}} , \quad (3)$$

where  $\mathcal{P}(\cdot)$  denotes the perceptual similarity measured by the LPIPS metric [48].

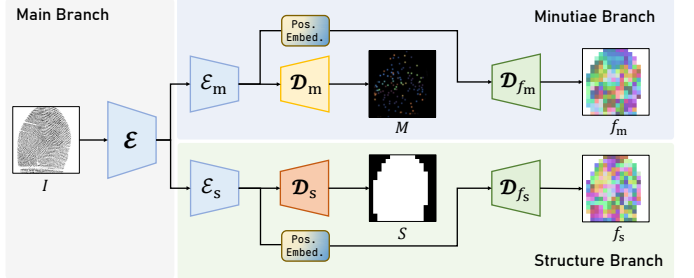


Fig. 6. The architecture illustration of FDRN.

#### D. Fixed-length Dense Representation Extraction

To handle various fingerprint foreground area and mitigate background interference, we adopt a three-dimensional dense representation, with two axes corresponding to spatial coordinates. Unlike previous approaches that compress the entire fingerprint into a global abstract one-dimensional vector, this representation retains local structural details and facilitates foreground-background separation via an associated validity mask that identifies meaningful fingerprint regions. Based on this design, we propose the Fixed-length Dense Representation Network (FDRN) to extract a fixed-length dense descriptor that captures both minutiae-related and structure-related features, thereby enhancing discriminative capability.

The FDRN is built upon ResNet-34 [49], with the first max-pooling layer removed to preserve fine-grained details. Furthermore, we modify it into a dual-branch structure to capture complementary aspects of the fingerprint representation. Since the input fingerprint images have been aligned to a canonical coordinate system through pose estimation, the dense descriptor space is also spatially aligned. To further enhance spatial awareness, we incorporate a classical 2D sinusoidal positional embedding module [50] into each dense representation decoder, enabling the network to extract more distinct and location-sensitive features. The network architecture is illustrated in Fig. 6.

Specifically, we formulate the two branches as multi-task learning modules. Given an input fingerprint image  $I \in \mathbb{R}^{1 \times H \times W}$ , the first branch (Minutiae branch) outputs a minutiae map  $M \in \mathbb{R}^{6 \times \frac{H}{2} \times \frac{W}{2}}$  [16], along with a fixed-length dense representation  $f_m \in \mathbb{R}^{D \times \frac{H}{16} \times \frac{W}{16}}$  that is related to the minutiae. The second branch (Structure branch) generates a foreground segmentation map  $S \in \mathbb{R}^{1 \times \frac{H}{16} \times \frac{W}{16}}$ , which corresponds to the spatial size of the dense descriptor, and produces a structure-aware representation  $f_s \in \mathbb{R}^{D \times \frac{H}{16} \times \frac{W}{16}}$  that focus on the foreground ridge patterns. The final fixed-length dense descriptor  $f \in \mathbb{R}^{2D \times \frac{H}{16} \times \frac{W}{16}}$  is obtained by concatenating the dense representations from both branches and applying the foreground mask as follows:

$$f = (f_s \oplus f_m) \odot S , \quad (4)$$

where  $\oplus$  stands for the concatenation and  $\odot$  represents the Hadamard product.

The loss functions for the representation extraction network consist of two main components: one for learning the dense representations and the other for the auxiliary tasks. For the

representation learning component, we adopt the CosFace loss [51] as a classification loss  $\mathcal{L}_{\text{cls}}$  to encourage each dense representations to acquire discriminative identity-related features. The two branches,  $f_m$  and  $f_s$ , are supervised independently, leading to a total classification loss of  $\mathcal{L}_{\text{cls}} = \mathcal{L}_{\text{cls}}^m + \mathcal{L}_{\text{cls}}^s$ . To further enhance the robustness of dense descriptors against variations in foreground coverage, intensity distribution, and local distortion, we introduce a local consistency loss  $\mathcal{L}_{\text{lc}}$  that enforces feature similarity across overlapping foreground regions of different impressions from the same identity. Specifically, we simulate an incomplete fingerprint  $I_{\text{inc}}$  by applying a binary mask derived from a real plain fingerprint onto a rolled fingerprint  $I_{\text{rol}}$ , followed by elastic deformation and intensity shifting to emulate natural variations. Specifically, the loss function is defined by:

$$\mathcal{L}_{\text{lc}} = \frac{1}{|S_{\text{inc} \cap \text{rol}}|} \sum_{(i,j) \in S_{\text{inc} \cap \text{rol}}} \|f^{\text{inc}}(i,j) - f^{\text{rol}}(i,j)\|_2^2, \quad (5)$$

where  $f^{\text{inc}}$  and  $f^{\text{rol}}$  denotes the dense descriptors extracted from  $I_{\text{inc}}$  and  $I_{\text{rol}}$  respectively.  $S_{\text{inc} \cap \text{rol}}$  represents the overlapping foreground regions.

For the auxiliary tasks, we supervise the network to predict both the minutiae map and the foreground mask. The auxiliary loss consists of a binary cross-entropy loss  $\mathcal{L}_{\text{mask}}$  for the mask prediction and a MSE loss  $\mathcal{L}_{\text{mnt}}$  for the minutiae map regression. The ground-truth minutiae maps and foreground masks are extracted using VeriFinger v12.0 [26]. The overall loss for the Fixed-length Dense Representation Network (FDRN) is defined as:

$$\mathcal{L}_{\text{FDRN}} = \mathcal{L}_{\text{cls}} + \lambda_{\text{ls}} \mathcal{L}_{\text{ls}} + \lambda_{\text{mask}} \mathcal{L}_{\text{mask}} + \lambda_{\text{mnt}} \mathcal{L}_{\text{mnt}}, \quad (6)$$

where we set  $\lambda_{\text{mask}} = 1$ ,  $\lambda_{\text{mnt}} = 0.01$ , and  $\lambda_{\text{ls}} = 0.00125$  to achieve roughly the same decreasing rate for these loss functions.

### E. Fingerprint Matching

In practical deployments, dense representations for all gallery fingerprints are extracted offline through the complete FLARE pipeline, including pose estimation, enhancement, and descriptor extraction. These fixed-length representations are then stored in a database for efficient matching.

During inference, a query fingerprint  $I_q$  undergoes the same processing steps. Given a 500 ppi query image  $I_q$  and a gallery image  $I_g$ , we first apply pose estimation and alignment, followed by cropping to  $512 \times 512$  pixels. The aligned images are then enhanced using two pose estimation methods and two enhancement strategies, producing four augmented versions of each image:  $\{(I_q^i, I_g^i) \mid i = 0, 1, 2, 3\}$ . To balance computational efficiency and matching accuracy, each enhanced image is downsampled to  $256 \times 256$  pixels before being input to the Fixed-length Dense Representation Network (FDRN), which produces dense descriptors  $f_q^i, f_g^i \in \mathbb{R}^{2D \times 16 \times 16}$  and foreground masks  $S_q^i, S_g^i \in \mathbb{R}^{1 \times 16 \times 16}$  (see Eq. 4). The matching score is computed by measuring the cosine similarity between the flattened dense representations  $f_q^{i'}, f_g^{i'} \in \mathbb{R}^{512D}$ , where only the overlapping foreground regions are considered.

TABLE I  
TRAINING CONFIGURATIONS OF THE BLOCKS IN FLARE. BS: BATCH SIZE, LR: LEARNING RATE.

Block	BS	LR	Epochs	GPU
Duan et al. [24]	64	$3.5 \times 10^{-4}$	80	1 × RTX 3090
Guan et al. [25]	64	$1 \times 10^{-3}$	80	1 × RTX 3090
UNetEnh	32	$1 \times 10^{-4}$	50	1 × RTX 3090
PriorEnh s1	12	$7 \times 10^{-5}$	40	6 × RTX 4090
PriorEnh s2	4	$1 \times 10^{-5}$	50	2 × RTX 3090
FDRN	24	$1 \times 10^{-4}$	200	1 × RTX 3090

Specifically, the score for the  $i$ -th fingerprint pair  $(I_q^i, I_g^i)$  is defined as:

$$\mathcal{M}^i(q, g) = \frac{f_q^{i'}^T \cdot f_g^{i'}}{\|f_q^i \odot S_g^i\|_F \|f_g^i \odot S_q^i\|_F}, \quad (7)$$

where  $\|\cdot\|_F$  stands for Frobenius norm. And the final matching score for fingerprint images  $(I_q, I_g)$  is obtained by taking the maximum over the four matching scores derived from different pose-enhancement combinations:

$$\mathcal{M}(q, g) = \max_{i \in \{0, 1, 2, 3\}} \mathcal{M}^i(q, g). \quad (8)$$

### F. Implementation Details

To improve generalization and prevent overfitting, we adopt a data augmentation strategy that simulates multiple impressions of the same finger. Specifically, we use the fingerprint distortion model proposed by Si et al. [21] to generate random distortion fields, which are applied to real fingerprints to synthesize impressions with varied geometric deformations. In addition, histogram matching adjusts the grayscale distribution of synthetic images to simulate a broader range of visual conditions. We also incorporate mild geometric transformations. For pose estimation and enhancement modules, we apply random translations in the range  $[-80, 80]$  pixels along both axes, and rotations within  $[-45^\circ, 45^\circ]$ . For FDRN training, we adopt smaller transformations with translations in  $[-10, 10]$  pixels and rotations in  $[-5^\circ, 5^\circ]$ . Furthermore, for training the enhancement modules, we adopt the simulated low-quality fingerprint strategy described in Sec. III-C, where realistic degradations are applied to high-quality prints to generate paired training data. The codebook size  $l_c$  is set to 4096, with an embedding dimension  $d_c$  of 3. The feature dimension  $D$  for the fixed-length dense representation is set to 6. Additional training details for each FLARE module are summarized in Tab. I, while full network hyperparameter settings are provided in the supplementary material.

## IV. EXPERIMENT

In this section, we first introduce the datasets used in our experiments, followed by the evaluation of FLARE's matching performance in comparison with representative fixed-length representation methods. We also present experiments analyzing the impact of pose estimation and enhancement, including their complementary effects. Finally, we conduct ablation studies and provide an in-depth analysis of the proposed fixed-length dense representation.

TABLE II  
FINGERPRINT DATASETS USED IN OUR WORK.

Type	Dataset	Sensor	Description	Usage	Genuine Pairs	Imposter Pairs
Rolled	NIST SD14	Inking	24,000 pairs of rolled fingerprints	train <sup>a</sup>	-	-
	NIST SD4	Inking	2,000 pairs of rolled fingerprints	test	2000	3,998,000
Plain	FVC2004 DB1A <sup>b</sup>	Optical	100 fingers $\times$ 8 impressions	test	2,800	4,950
	N2N Plain	Optical	2,000 pairs (plain and rolled fingerprints)	test	2,000	3,998,000
	DPF	Optical	776 rolled and 40,112 plain fingerprints with diverse poses	train <sup>c</sup>	-	-
Partial	FVC2002 DB3A <sup>b</sup>	Capacitive	100 fingers $\times$ 8 impressions	test	2,800	4,950
	FVC2006 DB1A <sup>d</sup>	Electric field	140 fingers $\times$ 12 impressions	test	9,240	9,730
Latent	NIST SD27 <sup>e</sup>	-	258 pairs (latent fingerprints from crime scene)	test	258	2,764,470
	THU Latent10K	-	10,458 pairs (latent fingerprints from crime scene)	test	10,458	109,359,306
Contactless	PolyU CL2CB <sup>f</sup>	Optical/Camera	336 fingers $\times$ 6 contact-based and contactless fingerprints	test	12,096	4,052,160

<sup>a</sup> It is used for training the FDRN, and the first 3,200 gallery fingerprints are also used to train the pose estimation module.

<sup>b</sup> The number of genuine pairs is  $100 \times \binom{8}{2} = 2,800$ , and the number of imposter pairs is  $\binom{100}{2} = 4,950$ .

<sup>c</sup> It is used to train both the pose estimation and fingerprint enhancement modules.

<sup>d</sup> The number of genuine pairs is  $140 \times \binom{12}{2} = 9,240$ , and the number of imposter pairs is  $\binom{140}{2} = 9,730$ .

<sup>e</sup> The gallery portion (10,458 plain or rolled fingerprints) of THU Latent10K is appended to the original gallery set.

<sup>f</sup> The number of genuine pairs is  $336 \times 6 \times 6 = 12,096$ , and the number of imposter pairs is  $336 \times 335 \times 6 \times 6 = 4,052,160$ .

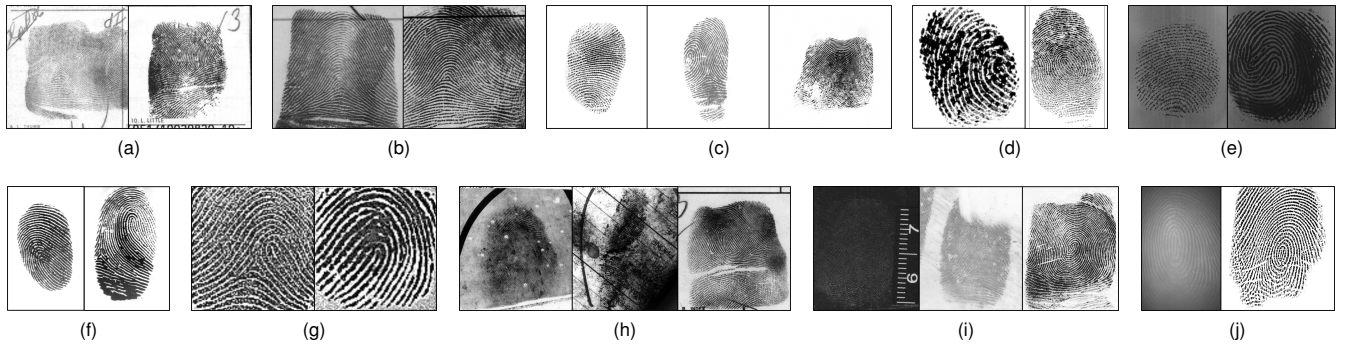


Fig. 7. Fingerprint examples from different fingerprint datasets (a) NIST SD14, (b) NIST SD4, (c) DPF, (d) N2N Plain, (e) FVC2002 DB3A, (f) FVC2004 DB1A, (g) FVC2006 DB1A, (h) NIST SD27, (i) THU Latent10K, (j) PolyU CL2CB. The input images are at 500 ppi, but have been rescaled in this figure to facilitate clearer visualization.

TABLE III  
DESCRIPTION OF THE COMPARED FIXED-LENGTH REPRESENTATION METHODS.

Approach	Preprocessing	Representation
DeepPrint [16]	STN alignment	Minutiae/Texture (1D)
AFRNet [17]	STN alignment	CNN/Transformer (1D)
MultiScale [19]	Pose alignment	Multi-region (1D)
FDD [32]	Pose alignment	Minutiae/Structure (dense)
FLARE	Dual Pose/Enh. <sup>‡</sup>	Minutiae/Structure (dense)

<sup>‡</sup> It stands for dual fingerprint pose alignment and dual fingerprint enhancement.

### A. Datasets

We employ a variety of fingerprint datasets in this work, covering multiple modalities including rolled, plain, partial, latent, and contactless fingerprints, collected using diverse sensors and under varying acquisition conditions. All fingerprint images not originally in 500 ppi resolution are rescaled to 500 ppi. Tab. II summarizes the details of all the datasets used in our experiments, and representative fingerprint samples from each are illustrated in Fig. 7.

For training, we use only high-quality rolled and plain fin-

gerprints to emphasize generalization capability. Specifically, we adopt the Diverse Pose Fingerprint (DPF) dataset [24], which contains 776 rolled fingerprints and 40,112 plain fingerprints with diverse pose variations, along with the first 3,200 rolled fingerprints from the gallery portion of NIST SD14, to train the pose estimation module. The same DPF dataset is also used to train the fingerprint enhancement modules, and the codebook for PriorEnh is constructed based on it as well. For training the fixed-length dense representation, we follow our previous conference work [32] and use the first 24,000 pairs of rolled fingerprints from NIST SD14. Additionally, 32,676 plain fingerprints from 633 fingers in DPF are randomly selected and combined with their segmentation masks to simulate incomplete fingerprints as described in Eq. 5. It is important to note that all training is performed exclusively on high-quality contact-based rolled or plain fingerprints, without exposure to other modalities. Evaluation is conducted directly on fingerprints of various types without fine-tuning.

To evaluate the generalization and robustness of our method, we conduct experiments on several benchmark and diverse fingerprint datasets covering a wide range of modalities. For the FVC benchmark, we select three representative datasets: FVC2002 DB3A, FVC2004 DB1A, and FVC2006 DB1A. For these datasets, we followed the same experimental settings for

TABLE IV

MATCHING ACCURACY (%) ON SEVERAL FINGERPRINT DATASETS. UNLESS OTHERWISE SPECIFIED, TAR@FAR = 0.1% IS REPORTED. BOLD INDICATES THE BEST PERFORMANCE, AND ITALIC DENOTES THE SECOND-BEST.

Method	NIST SD4		N2N Plain		FVC02 <sup>‡</sup>	FVC04 <sup>‡</sup>	FVC06 <sup>‡</sup>	PolyU <sup>‡</sup>	NIST SD27		THU Latent10K	
	Rank-1	TAR <sup>†</sup>	Rank-1	TAR <sup>†</sup>	TAR				Rank-1	TAR	Rank-1	TAR
DeepPrint [16]	98.65	95.95	79.45	71.60	60.36	85.07	77.85	53.41	24.03	33.33	57.71	68.44
MultiScale [19]	99.05	98.00	98.10	97.70	77.04	96.86	79.69	47.34	29.07	36.05	69.07	76.75
AFRNet [17]	97.45	94.70	96.80	96.05	83.68	98.61	<b>90.42</b>	70.13	31.78	41.86	68.91	78.65
FDD [32]	<b>99.75</b>	99.60	98.65	98.75	95.86	99.50	89.62	88.62	51.94	62.02	82.46	90.79
FLARE	<b>99.75</b>	<b>99.70</b>	<b>98.85</b>	<b>98.95</b>	<b>96.36</b>	<b>99.57</b>	89.95	<b>98.11</b>	<b>60.85</b>	<b>69.38</b>	<b>85.12</b>	<b>93.33</b>

<sup>†</sup> TAR@FAR=0.01%.

<sup>‡</sup> FVC02, FVC04, FVC06, and PolyU denote FVC2002 DB3A, FVC2004 DB1A, FVC2006 DB1A, and PolyU CL2CB, respectively. This naming convention is consistently used in Tab. VI and Tab. VIII.

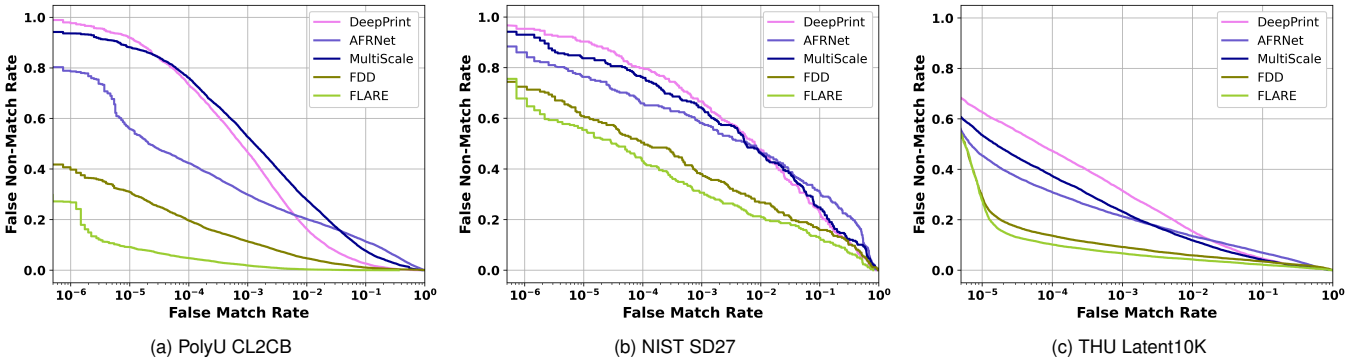


Fig. 8. DET curves for (a) contactless-to-contact matching on PolyU CL2CB, and (b, c) latent-to-contact matching on NIST SD27 and THU Latent10K, respectively.

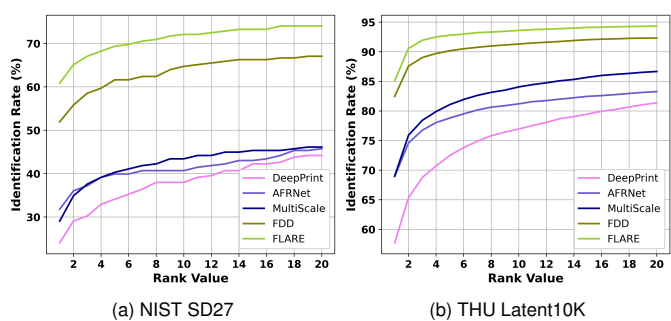


Fig. 9. CMC curves for latent-to-contact matching on (a) NIST SD27 and (b) THU Latent10K.

splitting the imposter and genuine pairs as used in previous works [7], [52]. The NIST SD302 dataset [53] contains 2,000 fingers from 200 subjects. We use subset U (2,000 rolled fingerprints) as the gallery, and combine subsets R and S (2,000 plain fingerprints) as the query, forming the N2N Plain. For evaluation on the NIST SD27 latent fingerprint dataset, we expand the gallery by including 10,458 rolled fingerprints from the gallery portion of our internal dataset, THU Latent10K. For the contactless-to-contact setting, we follow the preprocessing protocol of Cui et al. [54] on the PolyU CL2CB dataset [55], where contactless fingerprints are scaled to match the mean ridge period of contact-based fingerprints without applying any geometric warping.

### B. Fingerprint Matching Performance Comparison

We compare our method with several high-performing and representative fixed-length fingerprint matching approaches, including DeepPrint [16], AFRNet [17], MultiScale [19], and our previous conference work FDD [32]. A summary of the key characteristics of these methods is provided in Tab. III. Since the official implementations of DeepPrint [16] and AFRNet [17] are not publicly available, we reimplemented them to the best of our ability based on the details provided in their respective papers. For MultiScale [19] and FDD [32], which require fingerprint pose estimation as a preprocessing step, we employ the method of Duan et al. [24] to estimate the 2D pose for all corresponding experiments. All fingerprint representation extraction methods are trained using the same dataset and data augmentation strategies. For AFRNet and DeepPrint, however, we additionally apply random rotations within  $[-30^\circ, 30^\circ]$  during training to better facilitate the learning of their STN-based alignment modules. The evaluation metrics include Rank-1 accuracy for closed-set identification tasks, and True Accept Rates (TAR) at False Accept Rates (FAR) of 0.1% and 0.01% for open-set verification tasks. To provide a more comprehensive comparison of matching performance on challenging datasets such as latent fingerprints (which typically exhibit low image quality) and contactless fingerprints (which involve cross-modality matching), we plot the Detection Error Tradeoff (DET) curves for the relevant datasets, as shown in Fig. 8. In addition, we present the

Cumulative Match Characteristic (CMC) curves on latent fingerprints to evaluate closed-set identification performance, as shown in Fig. 9.

As shown in Tab. IV and Fig. 8–9, both FDD and FLARE demonstrate strong performance across a wide range of fingerprint types—including rolled, plain, partial, contactless, and latent—outperforming prior fixed-length methods based on one-dimensional descriptors [16], [17], [19] in most cases. This improvement can be attributed to our proposed fixed-length dense descriptors, which explicitly encode spatially localized fingerprint features, allowing the model to focus on foreground regions and suppress background noise. In contrast, one-dimensional descriptor approaches often rely on global aggregation without explicit modeling of foreground structures, making them more vulnerable to degraded inputs caused by noise or partial fingerprints.

Building upon FDD, FLARE further introduces fingerprint enhancement and incorporates multiple complementary pose estimation and enhancement strategies. These components not only improve the quality of the input images for descriptor extraction but also increase robustness against pose estimation inaccuracies. As a result, FLARE consistently achieves competitive or superior performance compared to FDD across all benchmarks. The benefits of enhancement are particularly pronounced in challenging scenarios. On fingerprints affected by significant noise or modality shifts—such as those in NIST SD27, THU Latent10K (latent), and PolyU CL2CB (contactless)—FLARE shows notable improvements, demonstrating enhanced ridge clarity and reduced background interference that translate to better matching accuracy.

### C. Analysis of Dense Representations

We conduct an ablation study of the fixed-length dense representation network. All experiments are conducted under the same configuration as FDD [32], using the pose estimation method of Duan et al. [24] without applying any enhancement. We evaluate three variants: (1) removing the minutiae branch (w/o Mnt. Branch), (2) merging the two branches into a single one that jointly handles auxiliary tasks and descriptor extraction (Combined Branch), and (3) removing the 2D positional embedding (w/o Pos. Embedding). All variants retain the same descriptor dimensionality  $f \in \mathbb{R}^{12 \times 16 \times 16}$  and are trained to convergence. As shown in Tab. V, excluding the minutiae branch leads to a notable performance drop in cross-modality matching, particularly on the contactless dataset PolyU CL2CB, underscoring the importance of the minutiae-aware representation in improving cross-modality matching generalization. Merging the branches reduces the overall representational capacity, especially under challenging conditions such as latent fingerprints. Finally, removing the positional embedding consistently impairs performance, highlighting its critical role in spatial encoding and matching reliability for degraded images.

To further validate the effectiveness of separately extracting minutiae-aware and structure-aware descriptors, we analyze the similarity distributions of the two branches. Specifically, we evaluate the matching scores between  $f_m$  and  $f_s$  extracted

TABLE V  
ABLATION EVALUATIONS ON EXTRACTION OF FIXED-LENGTH DENSE REPRESENTATION NETWORK (FDRN). TAR@FAR=0.1% IS REPORTED.

Ablations	NIST SD27		THU Latent10K		PolyU
	Rank-1	TAR	Rank-1	TAR	TAR
w/o Mnt. Branch	42.25	54.65	78.65	87.71	72.76
Combined Branch	43.02	53.49	78.69	88.34	87.76
w/o Pos. Embedding	44.96	55.43	80.92	88.99	88.09
None	51.94	62.02	82.46	90.79	88.62

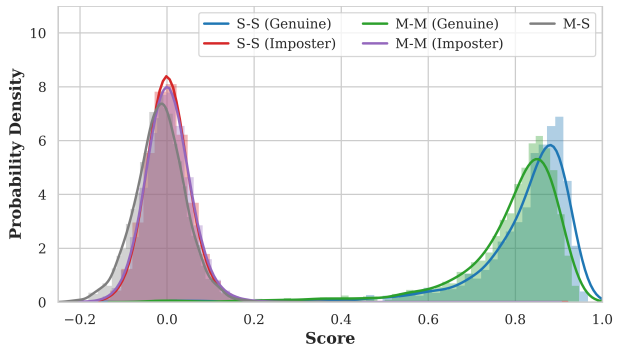


Fig. 10. Distribution of cosine similarity scores between different types of descriptor pairs on the N2N Plain dataset. “S-S” and “M-M” denote structure-to-structure and minutiae-to-minutiae descriptor matching, respectively, while “M-S” indicates cross-matching between the two branches extracted from the same fingerprint.

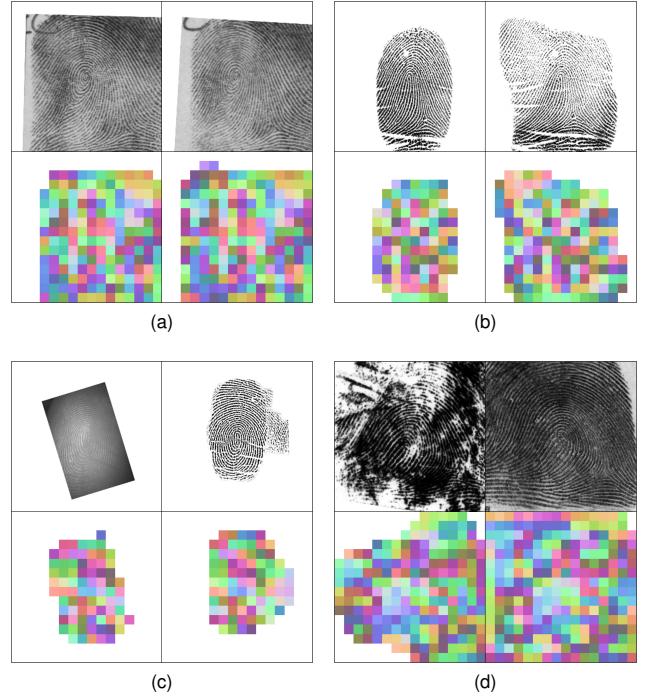


Fig. 11. Examples of the fixed-length dense representation extracted from genuine pairs of (a) NIST SD4, (b) N2N Plain, (c) PolyU CL2CB, (d) NIST SD27. The fingerprint images shown in the figure have been aligned based on their estimated poses.

from the same image, as well as genuine and imposter pairs of  $f_m$  (M-M) and  $f_s$  (S-S) on the N2N Plain dataset. The score distributions are illustrated in Fig. 10. We observe that

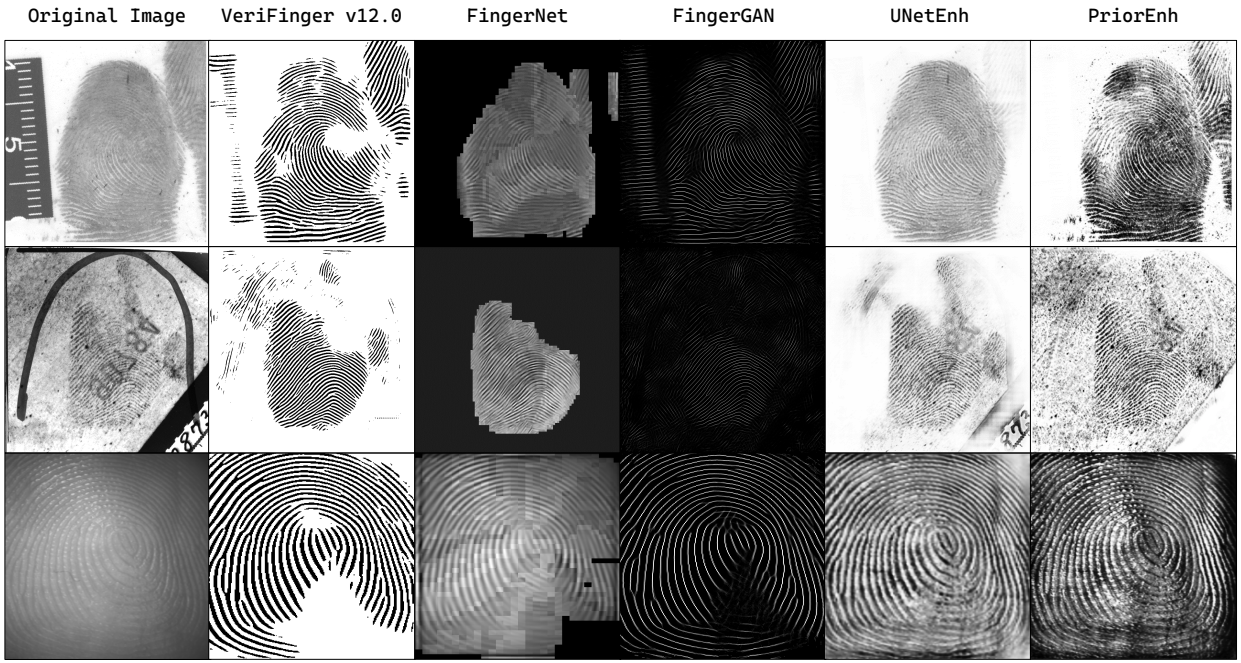


Fig. 12. Qualitative comparison of fingerprint enhancement results across different methods. Each row shows a representative fingerprint from THU Latent10K, NIST SD27, and PolyU CL2CB, respectively.

the similarity between  $f_m$  and  $f_s$  resembles that of imposter distributions, indicating that the two branches capture complementary information without redundancy.

To more intuitively illustrate the robustness of the dense descriptors in fingerprint representation, Fig. 11 shows visualizations of the dense representations extracted from genuine fingerprint pairs under different conditions. For rolled fingerprints (Fig. 11a), the representations are highly consistent across impressions. In plain fingerprint matching (Fig. 11b), strong correspondence is maintained in the overlapping regions. For contactless-to-contact matching (Fig. 11c), the representations demonstrate notable robustness against modality variations. In latent-to-rolled matching (Fig. 11d), the representations effectively suppress background noise and preserve structural consistency within valid ridge areas.

These results highlight the intrinsic robustness of the dense descriptor. Furthermore, we analyze how enhancement strategies contribute to quality improvement for more reliable descriptor extraction and matching (Sec. IV-D), and how pose estimation improves robustness to input pose variations, as detailed in the supplementary material.

#### D. Evaluation of Enhancement Methods

In this section, we compare our enhancement methods, UNetEnh and PriorEnh, with representative approaches including VeriFinger v12.0 [26], FingerNet [28], and FingerGAN [27]. For FingerNet and FingerGAN, we use the officially released pretrained models, while VeriFinger is evaluated using the commercial API we obtained through purchase. As shown in Fig. 12, results on three fingerprint types—latent (THU Latent10K, NIST SD27) and contactless (PolyU CL2CB)—demonstrate clear visual differences. VeriFinger and FingerGAN tend to misinterpret background

noise as ridge patterns, while FingerNet often exhibits blocky artifacts that compromise continuity. In contrast, our methods enhance contrast while preserving the original ridge structures, without introducing hallucinated textures. This structural fidelity contributes to better compatibility with descriptor extraction and ultimately improved matching performance.

We further evaluate how different enhancement methods affect the performance of descriptor-based matching. In this experiment, we fix the pose alignment method to that of Duan et al. [24] and use the fixed-length dense descriptor for representation, varying only the enhancement module to assess its impact on overall matching accuracy. Enhancement methods such as VeriFinger [26], FingerNet [28], and FingerGAN [27] have proven effective in restoring local ridge structures. However, they substantially modify the fingerprint modality by imposing strong texture priors or altering ridge patterns, which often introduce noise or blurring artifacts. As shown in Tab. VI, such modifications adversely affect the matching of dense representations due to their high sensitivity to global texture consistency, leading to consistent performance degradation across all evaluated datasets. In contrast, our proposed UNetEnh offers limited improvements on clean contact-based fingerprints but yields notable gains on noisy latent and contactless fingerprints. PriorEnh, which incorporates prior ridge information, further improves performance across both low-quality and high-quality datasets. We also evaluate a variant where the descriptor extraction is retrained on enhanced images corresponding to each enhancement method. The overall conclusions remain consistent, as detailed in the supplementary material. Overall, both UNetEnh and PriorEnh maintain stable accuracy on clean contact-based fingerprints while substantially boosting matching robustness under challenging conditions such as noise and modality gaps.

TABLE VI  
MATCHING PERFORMANCE (%) WITH DIFFERENT ENHANCEMENT METHODS. VALUES ARE REPORTED AS RELATIVE DIFFERENCES FROM THE ORIGINAL IMAGE BASELINE. UNLESS OTHERWISE SPECIFIED, TAR@FAR = 0.1% IS REPORTED.

Enh. Method	NIST SD4		N2N Plain		FVC02	FVC04	FVC06	PolyU	NIST SD27		THU Latent10K	
	Rank-1	TAR <sup>†</sup>	Rank-1	TAR <sup>†</sup>	TAR				Rank-1	TAR	Rank-1	TAR
Orginal Image	99.75	99.60	98.65	98.75	95.86	99.50	89.62	88.62	51.94	62.02	82.46	90.79
VeriFinger [26]	-0.90	-1.10	-1.35	-1.70	-0.11	-0.57	-3.07	-5.93	-4.65	-10.47	-5.22	-4.51
FingerNet [28]	-0.50	-0.50	-1.35	-1.70	-0.79	-1.07	-8.99	-2.22	-1.16	-1.94	-1.92	-1.57
FingerGAN [27]	-0.65	-0.75	-4.45	-5.75	-20.43	-4.82	-9.18	-9.66	-17.44	-15.90	-12.25	-9.69
UNetEnh	-0.10	-0.10	-0.30	-0.25	-0.29	-0.32	-1.22	+7.83	+5.81	+5.42	+0.60	+0.19
PriorEnh	0.00	+0.05	-0.05	-0.15	+0.07	-0.11	+0.01	+7.49	+4.26	+0.38	+0.74	+0.70

<sup>†</sup> TAR@FAR=0.01%.

TABLE VII  
CORRECT AND SPURIOUS MINUTIAE FOR 258 LATENT FINGERPRINTS IN NIST SD27 BEFORE AND AFTER ENHANCEMENT. MINUTIAE ARE EXTRACTED BY VERIFINGER V12.0 [26].

Enhancement Method	# Correct	# Spurious
Original Image	3,296	<b>8,784</b>
VeriFinger [26]	3,275	11,409
FingerNet [28]	3,675	16,937
FingerGAN [27]	3,156	62,336
UNetEnh	<b>3,933</b>	30,864
PriorEnh	3,764	23,872

Moreover, we evaluate ridge restoration quality using minutiae annotations from Feng et al. [42] on NIST SD27. Extracted minutiae are obtained by VeriFinger. As shown in Tab. VII, UNetEnh and PriorEnh recover the most correct minutiae, though they also introduce more spurious ones. This is mainly due to retained background textures when noise cannot be fully suppressed, which may mislead VeriFinger. Nonetheless, our applied dense representations remains robust by focusing on foreground regions.

#### E. Complementary Effects of Pose and Enhancement Strategies

This section analyzes the complementarity of dual pose estimation and enhancement strategies in FLARE and their contribution to improving descriptor matching performance. Tab. VI and Tab. VII show that UNetEnh and PriorEnh exhibit different strengths in recovering ridge details and supporting descriptor extraction across varying image conditions. For pose estimation, Fig. 13 illustrates that when individual methods fail due to different types of estimation errors, fusing their results can effectively correct misalignments and recover the true match, thereby improving the overall matching accuracy.

Building on these intuitive examples, we now present quantitative results to demonstrate the incremental benefits brought by combining pose estimation and enhancement strategies. Tab. VIII presents a step-by-step quantitative evaluation across various fingerprint datasets. Starting from the baseline setup using a single pose estimation and no enhancement, we incrementally incorporate different pose estimators and enhancement modules. As shown in the table, each component

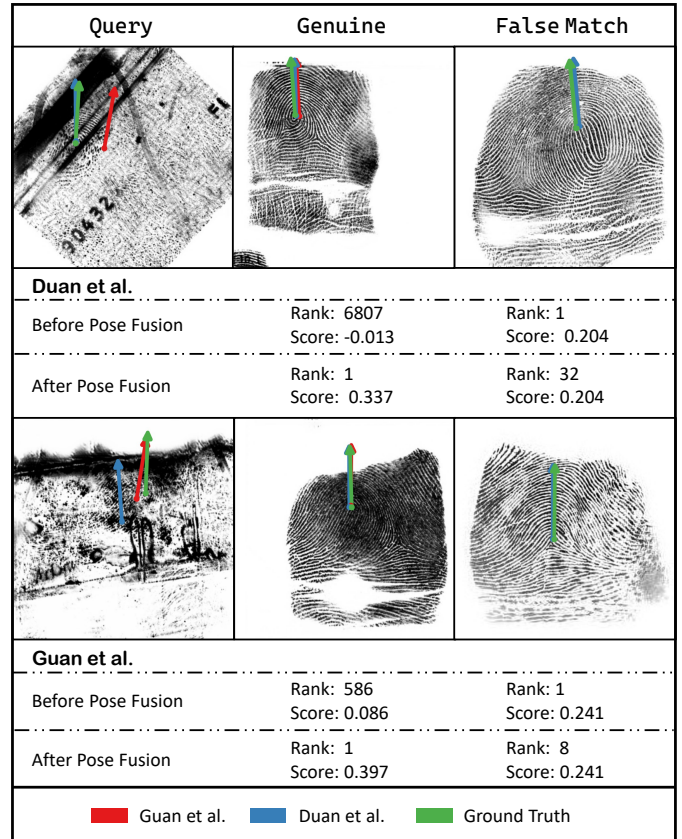


Fig. 13. Illustration of the effectiveness of pose fusion. The top and bottom examples show two query cases with their genuine and false matches. Arrows indicate pose estimation from Duan et al. [24] (blue), Guan et al. [25] (red), and the ground truth (green).

contributes to performance gains on multiple datasets. The final configuration, combining both Duan et al. [24] and Guan et al. [25] for pose estimation, along with both UNetEnh and PriorEnh for enhancement, achieves the best results across all evaluation sets. These findings confirm that the complementary nature of the selected methods leads to more robust and accurate fingerprint matching under diverse conditions.

## V. DISCUSSIONS

Although FLARE achieves state-of-the-art performance on multiple fingerprint datasets, there is still room for improve-

TABLE VIII

MATCHING ACCURACY (%) ON SEVERAL FINGERPRINT DATASETS WITH DIFFERENT METHODS COMBINATIONS. TAR@FAR = 0.1% IS REPORTED.

Pose Estimation		Enhancement		FVC02	FVC04	FVC06	PolyU	NIST SD27		THU Latent10K	
Duan [24]	Guan [25]	PriorEnh	UNetEnh	TAR				Rank-1	TAR	Rank-1	TAR
✓				95.86	99.50	89.52	88.62	51.94	62.02	82.46	90.79
✓		✓		95.93	99.39	89.63	96.11	56.20	62.40	83.20	91.49
✓		✓	✓	96.25	99.36	89.03	97.28	59.69	65.89	83.84	92.04
	✓			91.32	<b>99.57</b>	88.11	88.17	52.71	65.12	82.94	91.46
	✓	✓		93.21	99.36	88.16	95.98	53.49	62.79	83.75	92.10
	✓	✓	✓	93.75	99.39	87.35	97.07	57.75	66.28	83.95	91.98
✓	✓	✓	✓	<b>96.36</b>	<b>99.57</b>	<b>89.95</b>	<b>98.11</b>	<b>60.85</b>	<b>69.38</b>	<b>85.12</b>	<b>93.33</b>

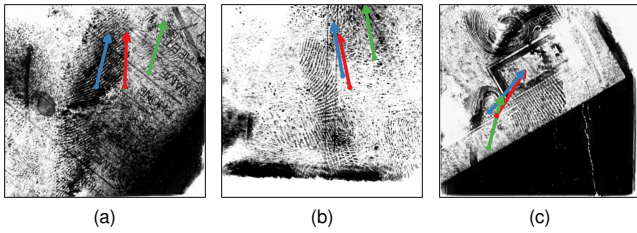


Fig. 14. Examples of erroneous pose estimation and enhancement with insufficient background suppression. Pose predictions are based on the original fingerprint images, and the orientation arrows follow the same definition as in Fig. 13.

ment. As shown in Fig. 14, current pose estimation methods can fail when fingerprints are severely degraded or incomplete, such as in latent prints, leading to incorrect alignment and failed matching. While our enhancement modules improve ridge clarity without introducing false ridge patterns, they may sharpen background textures. This can lead to over-detection of spurious minutiae, as shown in Tab. VII, and may interfere with pose estimation, particularly for local voting-based methods, when applied to enhanced images. Therefore, FLARE estimates pose from the original images. Future work will explore more robust pose estimation methods for damaged fingerprints and enhance the denoising ability of the enhancement network.

Regarding the dense descriptor, its spatial sensitivity significantly contributes to high matching accuracy once fingerprint alignment is achieved. However, in cases with minimal overlapping regions—such as partially captured fingerprints—this spatial rigidity may introduce matching ambiguity, potentially leading to incorrect identification when non-mated fingerprints share similar local patterns. To address this, we plan to enhance the fixed-length dense representation framework with overlap-aware strategies that take the extent of the overlapping area into account, improving robustness in more general cases.

## VI. CONCLUSION

In this paper, we propose FLARE, a fingerprint matching framework that integrates pose estimation, enhancement, and dense fixed-length descriptor extraction. FLARE standardizes fingerprint alignment through pose estimation, enhances ridge clarity while preserving structural fidelity, and extracts spatially aligned dense descriptors for robust matching. Beyond

proposing an effective framework, this work systematically explores and evaluates the collaborative effects of combining multiple pose estimation and enhancement strategies on fixed-length fingerprint representations. Experimental results on various types of fingerprints demonstrate that FLARE consistently achieves strong matching performance. The proposed enhancement modules, UNetEnh and PriorEnh, further improve matching accuracy, particularly on low-quality and contactless fingerprints. Moreover, the integration of multiple pose estimation and enhancement methods is shown to effectively improve matching performance across diverse fingerprint conditions. Overall, FLARE establishes a unified and scalable solution for fixed-length fingerprint representation and matching across diverse conditions, providing a practical foundation for reliable and accurate fingerprint recognition in real-world applications.

## REFERENCES

- [1] D. Maltoni, D. Maio, A. K. Jain, and J. Feng, *Handbook of Fingerprint Recognition*, 3rd ed. Springer Nature, Cham, Switzerland, 2022.
- [2] A. Jain, A. Ross, and S. Prabhakar, “An introduction to biometric recognition,” *IEEE Transactions on Circuits and Systems for Video Technology*, vol. 14, no. 1, pp. 4–20, 2004.
- [3] A. K. Jain, S. Prabhakar, L. Hong, and S. Pankanti, “FingerCode: A filterbank for fingerprint representation and matching,” in *Proceedings of the IEEE/CVF Conference on Computer Vision and Pattern Recognition*, vol. 2. IEEE, 1999, pp. 187–193.
- [4] Y. Wang, J. Hu, and D. Phillips, “A fingerprint orientation model based on 2D Fourier expansion (FOMFE) and its application to singular-point detection and fingerprint indexing,” *IEEE Transactions on Pattern Analysis and Machine Intelligence*, vol. 29, no. 4, pp. 573–585, 2007.
- [5] A. Kumar and Y. Zhou, “Contactless fingerprint identification using level zero features,” in *Proceedings of the IEEE/CVF Conference on Computer Vision and Pattern Recognition WorkShop*, 2011, pp. 114–119.
- [6] J. Bringer and V. Despiegel, “Binary feature vector fingerprint representation from minutiae vicinities,” in *2010 Fourth IEEE International Conference on Biometrics: Theory, Applications and Systems*, 2010, pp. 1–6.
- [7] R. Cappelli, M. Ferrara, and D. Maltoni, “Minutia Cylinder-Code: A new representation and matching technique for fingerprint recognition,” *IEEE Transactions on Pattern Analysis and Machine Intelligence*, vol. 32, no. 12, pp. 2128–2141, 2010.
- [8] Z. He, J. Zhang, L. Pang, and E. Liu, “PFVNet: A partial fingerprint verification network learned from large fingerprint matching,” *IEEE Transactions on Information Forensics and Security*, vol. 17, pp. 3706–3719, 2022.
- [9] Y. Qiu, H. Chen, X. Dong, Z. Lin, I. Yi Liao, M. Tistarelli, and Z. Jin, “Ifvit: Interpretable fixed-length representation for fingerprint matching via vision transformer,” *IEEE Transactions on Information Forensics and Security*, vol. 20, pp. 559–573, 2025.

- [10] X. Guan, Z. Pan, J. Feng, and J. Zhou, "Joint identity verification and pose alignment for partial fingerprints," *IEEE Transactions on Information Forensics and Security*, vol. 20, pp. 249–263, 2025.
- [11] K. Cao and A. K. Jain, "Automated latent fingerprint recognition," *IEEE Transactions on Pattern Analysis and Machine Intelligence*, vol. 41, no. 4, pp. 788–800, 2019.
- [12] H. İ. Öztürk, B. Selbes, and Y. Artan, "MinNet: Minutia patch embedding network for automated latent fingerprint recognition," in *2022 IEEE/CVF Conference on Computer Vision and Pattern Recognition Workshops*, 2022, pp. 1626–1634.
- [13] Z. Pan, Y. Duan, X. Guan, J. Feng, and J. Zhou, "Latent fingerprint matching via dense minutia descriptor," in *2024 IEEE International Joint Conference on Biometrics (IJCB)*, 2024, pp. 1–10.
- [14] K. Cao and A. K. Jain, "Fingerprint indexing and matching: An integrated approach," in *2017 IEEE International Joint Conference on Biometrics*, 2017, pp. 437–445.
- [15] D. Song and J. Feng, "Fingerprint indexing based on pyramid deep convolutional feature," in *2017 IEEE International Joint Conference on Biometrics (IJCB)*, 2017, pp. 200–207.
- [16] J. J. Engelsma, K. Cao, and A. K. Jain, "Learning a fixed-length fingerprint representation," *IEEE Transactions on Pattern Analysis and Machine Intelligence*, vol. 43, no. 6, pp. 1981–1997, 2021.
- [17] S. A. Grosz and A. K. Jain, "AFR-Net: Attention-driven fingerprint recognition network," *IEEE Transactions on Biometrics, Behavior, and Identity Science*, vol. 6, no. 1, pp. 30–42, 2024.
- [18] ——, "Latent fingerprint recognition: Fusion of local and global embeddings," *IEEE Transactions on Information Forensics and Security*, vol. 18, pp. 5691–5705, 2023.
- [19] S. Gu, J. Feng, J. Lu, and J. Zhou, "Latent fingerprint indexing: Robust representation and adaptive candidate list," *IEEE Transactions on Information Forensics and Security*, vol. 17, pp. 908–923, 2022.
- [20] Y. Zhang, R. Zhao, Z. Zhao, N. Ramakrishnan, M. Aggarwal, G. Medioni, and Q. Ji, "Robust partial fingerprint recognition," in *Proceedings of the IEEE/CVF Conference on Computer Vision and Pattern Recognition*, 2023, pp. 1011–1020.
- [21] X. Si, J. Feng, J. Zhou, and Y. Luo, "Detection and rectification of distorted fingerprints," *IEEE Transactions on Pattern Analysis and Machine Intelligence*, vol. 37, no. 3, pp. 555–568, 2015.
- [22] J. Ouyang, J. Feng, J. Lu, Z. Guo, and J. Zhou, "Fingerprint pose estimation based on faster r-cnn," in *2017 IEEE International Joint Conference on Biometrics (IJCB)*, 2017, pp. 268–276.
- [23] Q. Yin, J. Feng, J. Lu, and J. Zhou, "Joint estimation of pose and singular points of fingerprints," *IEEE Transactions on Information Forensics and Security*, vol. 16, pp. 1467–1479, 2021.
- [24] Y. Duan, J. Feng, J. Lu, and J. Zhou, "Estimating fingerprint pose via dense voting," *IEEE Transactions on Information Forensics and Security*, vol. 18, pp. 2493–2507, 2023.
- [25] X. Guan, Z. Pan, J. Feng, and J. Zhou, "Finger pose estimation for under-screen fingerprint sensor," *arXiv preprint arXiv:2505.02481*, 2025.
- [26] Neurotechnology. VeriFinger SDK. Accessed: Apr. 18, 2025. [Online]. Available: <https://www.neurotechnology.com/verifinger.html>
- [27] Y. Zhu, X. Yin, and J. Hu, "FingerGAN: A constrained fingerprint generation scheme for latent fingerprint enhancement," *IEEE Transactions on Pattern Analysis and Machine Intelligence*, vol. 45, no. 7, pp. 8358–8371, 2023.
- [28] Y. Tang, F. Gao, J. Feng, and Y. Liu, "FingerNet: An unified deep network for fingerprint minutiae extraction," in *2017 IEEE International Joint Conference on Biometrics*. IEEE, 2017, pp. 108–116.
- [29] X. Huang, P. Qian, and M. Liu, "Latent fingerprint image enhancement based on progressive generative adversarial network," in *2020 IEEE/CVF Conference on Computer Vision and Pattern Recognition Workshops (CVPRW)*, 2020, pp. 3481–3489.
- [30] O. Ronneberger, P. Fischer, and T. Brox, "U-net: Convolutional networks for biomedical image segmentation," in *Medical image computing and computer-assisted intervention-MICCAI 2015: 18th international conference, Munich, Germany, October 5-9, 2015, proceedings, part III* 18. Springer, 2015, pp. 234–241.
- [31] A. van den Oord, O. Vinyals, and K. Kavukcuoglu, "Neural discrete representation learning," in *Proceedings of the 31st International Conference on Neural Information Processing Systems*, ser. NIPS'17. Red Hook, NY, USA: Curran Associates Inc., 2017, p. 6309–6318.
- [32] Z. Pan, Y. Duan, J. Feng, and J. Zhou, "Fixed-length dense descriptor for efficient fingerprint matching," in *2024 IEEE International Workshop on Information Forensics and Security (WIFS)*, 2024, pp. 1–6.
- [33] D. Song and J. Feng, "Fingerprint indexing based on pyramid deep convolutional feature," in *2017 IEEE International Joint Conference on Biometrics*. IEEE, 2017, pp. 200–207.
- [34] D. Song, Y. Tang, and J. Feng, "Aggregating minutia-centred deep convolutional features for fingerprint indexing," *Pattern Recognition*, vol. 88, pp. 397–408, 2019.
- [35] S. Wu, B. Liu, Z. Wang, Z. Jia, and J. Feng, "Minutiae-awarely learning fingerprint representation for fingerprint indexing," in *2022 IEEE International Joint Conference on Biometrics*, pp. 1–8.
- [36] K. Nilsson and J. Bigun, "Localization of corresponding points in fingerprints by complex filtering," *Pattern Recognition Letters*, vol. 24, no. 13, pp. 2135–2144, 2003.
- [37] X. Jiang, M. Liu, and A. Kot, "Reference point detection for fingerprint recognition," in *Proceedings of the 17th International Conference on Pattern Recognition, 2004. ICPR 2004*, vol. 1, 2004, pp. 540–543 Vol.1.
- [38] R. Cappelli and D. Maltoni, "On the spatial distribution of fingerprint singularities," *IEEE Transactions on Pattern Analysis and Machine Intelligence*, vol. 31, no. 4, pp. 742–448, 2009.
- [39] X. Yang, J. Feng, and J. Zhou, "Localized dictionaries based orientation field estimation for latent fingerprints," *IEEE Transactions on Pattern Analysis and Machine Intelligence*, vol. 36, no. 5, pp. 955–969, 2014.
- [40] S. Gu, J. Feng, J. Lu, and J. Zhou, "Efficient rectification of distorted fingerprints," *IEEE Transactions on Information Forensics and Security*, vol. 13, no. 1, pp. 156–169, 2018.
- [41] R. Cappelli, D. Maio, and D. Maltoni, "Semi-automatic enhancement of very low quality fingerprints," in *2009 Proceedings of 6th International Symposium on Image and Signal Processing and Analysis*, 2009, pp. 678–683.
- [42] J. Feng, J. Zhou, and A. K. Jain, "Orientation field estimation for latent fingerprint enhancement," *IEEE Transactions on Pattern Analysis and Machine Intelligence*, vol. 35, no. 4, pp. 925–940, 2013.
- [43] C. Yao, X. Bai, W. Liu, Y. Ma, and Z. Tu, "Detecting texts of arbitrary orientations in natural images," in *2012 IEEE Conference on Computer Vision and Pattern Recognition*, 2012, pp. 1083–1090.
- [44] A. de Sá Soares, R. B. das Neves Junior, and B. L. D. Bezerra, "Bid dataset: a challenge dataset for document processing tasks," in *Conference on Graphics, Patterns and Images (SIBGRAPI)*. SBC, 2020, pp. 143–146.
- [45] L. Deng, "The mnist database of handwritten digit images for machine learning research," *IEEE Signal Processing Magazine*, vol. 29, no. 6, pp. 141–142, 2012.
- [46] A. v. d. Oord, N. Kalchbrenner, O. Vinyals, L. Espeholt, A. Graves, and K. Kavukcuoglu, "Conditional image generation with pixelcnn decoders," in *Proceedings of the 30th International Conference on Neural Information Processing Systems*, ser. NIPS'16. Red Hook, NY, USA: Curran Associates Inc., 2016, pp. 4797–4805.
- [47] X. Wang, K. Yu, C. Dong, and C. C. Loy, "Recovering realistic texture in image super-resolution by deep spatial feature transform," in *Proceedings of the IEEE conference on computer vision and pattern recognition*, 2018, pp. 606–615.
- [48] R. Zhang, P. Isola, A. A. Efros, E. Shechtman, and O. Wang, "The unreasonable effectiveness of deep features as a perceptual metric," in *2018 IEEE/CVF Conference on Computer Vision and Pattern Recognition*, 2018, pp. 586–595.
- [49] K. He, X. Zhang, S. Ren, and J. Sun, "Deep residual learning for image recognition," in *Proceedings of the IEEE conference on computer vision and pattern recognition*, 2016, pp. 770–778.
- [50] A. Vaswani, N. Shazeer, N. Parmar, J. Uszkoreit, L. Jones, A. N. Gomez, Ł. Kaiser, and I. Polosukhin, "Attention is all you need," *Advances in Neural Information Processing Systems*, vol. 30, 2017.
- [51] H. Wang, Y. Wang, Z. Zhou, X. Ji, D. Gong, J. Zhou, Z. Li, and W. Liu, "Cosface: Large margin cosine loss for deep face recognition," in *Proceedings of the IEEE conference on computer vision and pattern recognition*, 2018, pp. 5265–5274.
- [52] Y. Su, J. Feng, and J. Zhou, "Fingerprint indexing with pose constraint," *Pattern Recognition*, vol. 54, pp. 1–13, 2016.
- [53] G. Fiumara, P. Flanagan, J. Grantham, K. Ko, K. Marshall, M. Schwarz, E. Tabassi, B. Woodgate, and C. Boehnen, "National institute of standards and technology special database 302: Nail to nail fingerprint challenge," *Technical Note 2007, National Institute of Standards and Technology*, 2018.
- [54] Z. Cui, J. Feng, and J. Zhou, "Monocular 3D fingerprint reconstruction and unwarping," *IEEE Transactions on Pattern Analysis and Machine Intelligence*, vol. 45, no. 7, pp. 8679–8695, 2023.
- [55] F. Liu and D. Zhang, "3D fingerprint reconstruction system using feature correspondences and prior estimated finger model," *Pattern Recognition*, vol. 47, no. 1, pp. 178–193, 2014.

## Supplementary Material

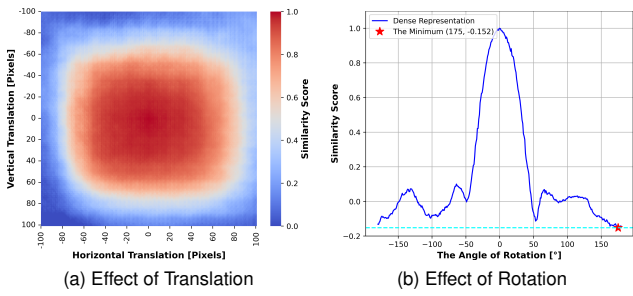


Fig. 15. The effect of pose variations on dense representations.

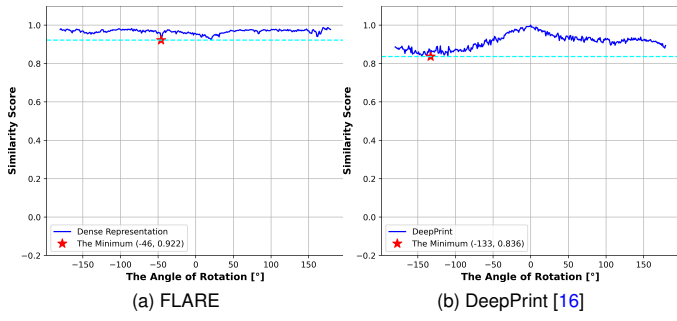


Fig. 16. The effect of rotation variations on (a) FLARE and (b) DeepPrint [16].

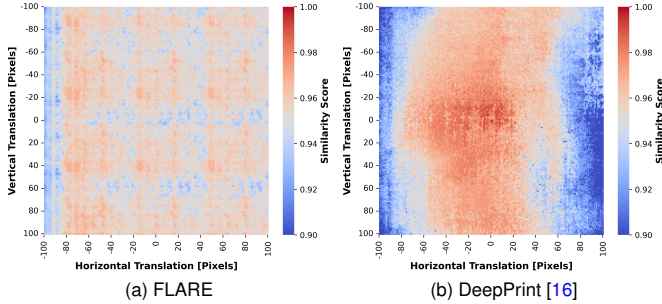


Fig. 17. The effect of translation variations on (a) FLARE and (b) DeepPrint [16].

## VII. DETAILED NETWORK STRUCTURE AND HYPERPARAMETER SETTINGS FOR PRIORENH AND FDRN

Tab. IX presents the hyperparameter settings for PriorEnh. Both  $E_H$  in the first stage and  $E_L$  in the second stage share the same architecture, while  $D_H$  corresponds to the symmetric UNet-based upsampling architecture. The detailed structure of FDRN is shown in Tab. X.

## VIII. EXPERIMENTS

### A. Robustness to 2D Pose Variations

Variations in the 2D pose of fingerprint images can affect descriptor extraction and thus impact matching accuracy. Since our dense descriptor is defined in a canonical fingerprint coordinate system with embedded spatial encoding, it is inherently sensitive to large pose deviations. To evaluate this, we select a low-quality, limited-area example from the N2N Plain

dataset (left image of Fig. 7d) and apply controlled translation and rotation. As shown in Fig. 15a, the descriptor exhibits moderate robustness to translation—likely due to the inherent shift tolerance of CNNs—but suffers a sharp performance drop under rotation (Fig. 15b). These results underscore the need for accurate pose alignment, which we address using precise pose estimation strategies in our framework.

In FLARE, pose robustness is achieved through explicit alignment using a pretrained pose estimation module, whereas methods like DeepPrint [16] rely on data augmentation to improve the robustness of descriptor extraction during training. To compare these strategies, we evaluate FLARE using the pose estimation method of Guan et al. [25] together with the original FDD [32], and compare it against DeepPrint [16]. For a fair comparison, both models are trained with the same extensive pose augmentation settings, including random rotations in  $[-180^\circ, 180^\circ]$  and translations of up to  $\pm 100$  pixels. Notably, the FDD model remains unchanged and does not benefit from augmented training. As shown in Fig. 16, FLARE maintains high descriptor similarity scores across a wide range of rotations ( $-180^\circ$  to  $180^\circ$ ), while DeepPrint shows a clear performance drop as the rotation angle increases. A similar trend is observed in Fig. 17, where FLARE demonstrates stronger translation robustness compared to DeepPrint. These results demonstrate that explicit pose correction leads to greater robustness than relying on large pose augmentation during descriptor training. Considering that extreme pose variations are uncommon in practical applications, all other experiments in this paper adopt the augmentation strategy described in Sec. III-F.

### B. More Evaluated Results on Fingerprint Matchings

Fig. 18 presents additional DET curves comparing all methods on rolled, plain, and partial fingerprint matching tasks. The results consistently demonstrate that FLARE outperforms the other methods across nearly all evaluated datasets.

### C. More Evaluated Results about Enhancement Methods

In the main text, we evaluated the performance of the Fixed-Length Dense Descriptor (FDD) [32] trained on original fingerprint images when applied to various enhanced images. Here, we further assess the performance of FDD models retrained using images enhanced by their corresponding methods. This is based on the assumption that both UNetEnh and PriorEnh perform enhancement in the original image domain, and thus should still use descriptor extraction networks trained on original images. As shown in Table XI, our proposed enhancement method demonstrates superior performance compared to the other enhancement approaches. When FDDs are retrained using images enhanced by their corresponding methods, performance improves on high-quality datasets such as NIST SD4, N2N Plain, and FVC2004 DB1A, compared to using the original FDD model trained solely on unenhanced images. However, on more challenging datasets—such as partial, latent, and contactless fingerprints—the retrained models

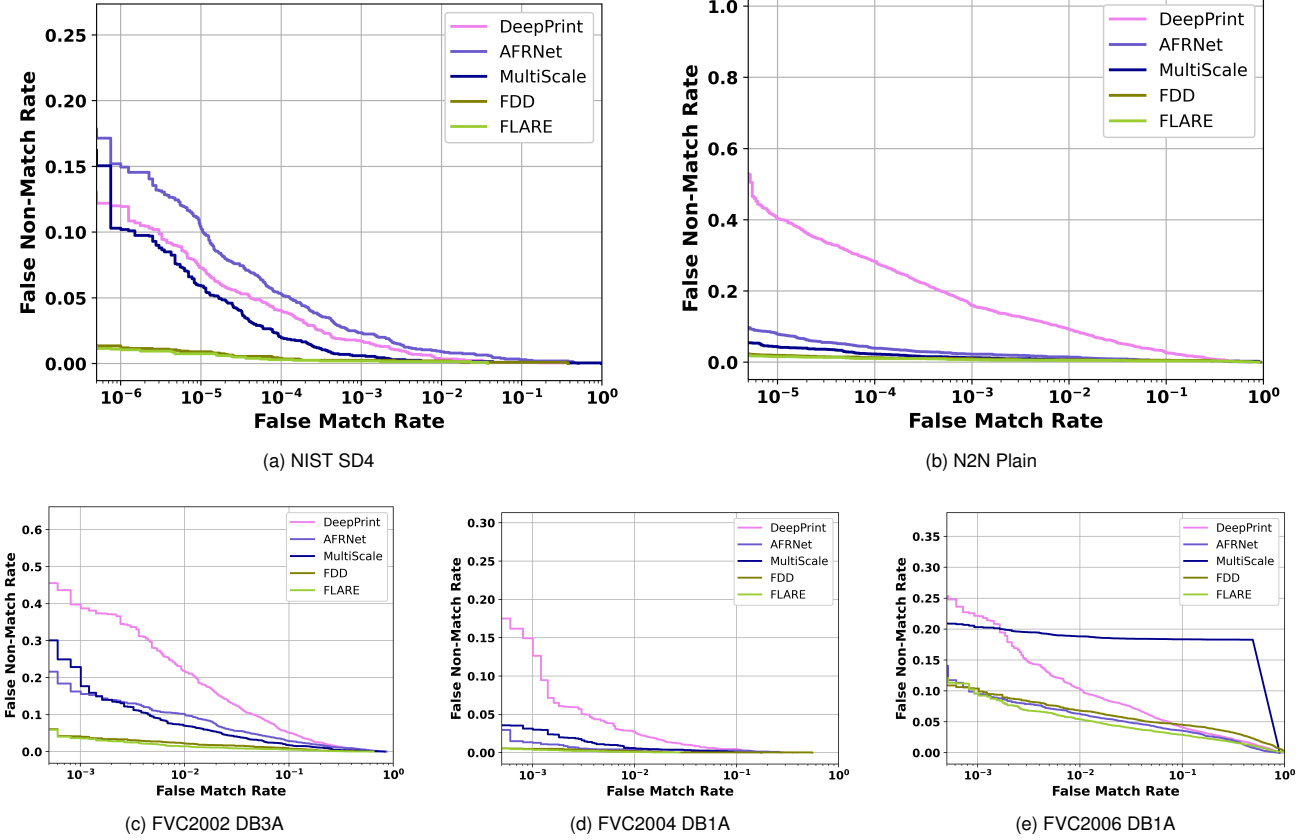


Fig. 18. Open-set identification performance of all methods, presented with DET curves for (a) rolled fingerprints matching on NIST SD4, (b, d) plain fingerprints matching on N2N Plain and FVC2004 DB1A, and (c, e) partial fingerprints matching on FVC2002 DB3A and FVC2006 DB1A, respectively.

TABLE IX  
THE HYPERPARAMETERS FOR THE PRIORENH.

Settings	PriorEnh 512 × 512
Compression Ratio	4
Latent Feature Shape	$128 \times 128 \times 3$
Codebook Length $l_c$	4096
Channels	64
Depth	2
Channel Multiplier	1,2,4
Attention resolutions	16
GatedPixelCNN Embedding dim	64

often perform worse than those trained on original images. Furthermore, for all evaluated datasets, these enhancement-specific models [26]–[28] still fail to surpass the performance achieved by applying the original model directly to unenhanced images. In contrast, our proposed enhancement method consistently improves matching accuracy across both high-quality and challenging datasets.

TABLE X  
DETAILED NETWORK STRUCTURE OF FDRN

$\mathcal{E}$			
Type	Output Size (spatial scales, channels)		# of Layer
7 × 7 Conv. Layer	/2, 64		1
3 × 3 Residue Block	1, 64		3
3 × 3 Residue Block	/2, 128		4
$\mathcal{E}_m \setminus \mathcal{E}_s$			
Type	Output Size (spatial scales, channels)		# of Layer
3 × 3 Residue Block <sup>a</sup>	/2, 256		6
3 × 3 Residue Block <sup>b</sup>	/2, 512		3
$\mathcal{D}_m$			
Type	Output Size (spatial scales, channels)		# of Layer
3 × 3 Conv. Layer	1, 128		6
4 × 4 Deconv. Layer	2, 64		2
3 × 3 Conv. Layer	1, 6		1
$\mathcal{D}_s$			
Type	Output Size (spatial scales, channels)		# of Layer
3 × 3 Conv. Layer	1, 512		1
1 × 1 Conv. Layer	1, 1		1
$\mathcal{D}_{fm} \setminus \mathcal{D}_{fs}$			
Type	Output Size (spatial scales, channels)		# of Layer
3 × 3 Conv. Layer	1, 512		1
1 × 1 Conv. Layer	1, 6		1

<sup>a</sup>  $\mathcal{D}_m$  connects from here.

<sup>b</sup> The branches for  $\mathcal{D}_s$  and  $\mathcal{D}_{fm} \setminus \mathcal{D}_{fs}$  connect from here.

TABLE XI

MATCHING PERFORMANCE (%) WITH DIFFERENT ENHANCEMENT METHODS. FDD [32] IS RETRAINED BASED ON THE ENHANCEMENT IMAGES. VALUES ARE REPORTED AS RELATIVE DIFFERENCES FROM THE ORIGINAL IMAGE BASELINE. UNLESS OTHERWISE SPECIFIED, TAR@FAR = 0.1% IS REPORTED.

Enh. Method	NIST SD4		N2N Plain		FVC02	FVC04	FVC06	PolyU	NIST SD27		THU Latent10K	
	Rank-1	TAR <sup>†</sup>	Rank-1	TAR <sup>†</sup>					Rank-1	TAR	Rank-1	TAR
Orginal Image	99.75	99.60	98.65	98.75	95.86	99.50	89.62	88.62	51.94	62.02	82.46	90.79
VeriFinger*[26]	-0.35	-0.55	-0.95	-1.20	-5.5	-0.68	-11.03	-15.41	-15.51	-19.38	-7.78	-6.55
FingerNet*[28]	-0.30	-0.10	-0.30	-0.55	-4.72	-0.68	-11.03	-19.75	-6.59	-4.27	-4.36	-3.71
FingerGAN*[27]	-0.25	-0.10	-0.30	-0.55	-21.68	-2.57	-37.48	-10.59	-7.75	-9.69	-5.79	-4.83
UNetEnh	-0.10	-0.10	-0.30	-0.25	-0.29	-0.32	-1.22	+7.83	+5.81	+5.42	+0.60	+0.19
PriorEnh	0.00	+0.05	-0.05	-0.15	+0.07	-0.11	+0.01	+7.49	+4.26	+0.38	+0.74	+0.70

<sup>†</sup> TAR@FAR=0.01%.

\* The FDD [32] is retrained using images enhanced by each corresponding method, while the training set remains the same—24,000 pairs of rolled fingerprints from the NIST SD14 dataset.